applied sciences

MDPI

Article

Furfural Oxidation on Gold Supported on MnO_2: Influence of the Support Structure on the Catalytic Performances

Camila Palombo Ferraz [1,2], Anderson Gabriel Marques Da Silva [2], Thenner Silva Rodrigues [2], Pedro Henrique Cury Camargo [2], Sébastien Paul [1] and Robert Wojcieszak [1,*]

1 Univ. Lille, CNRS, Centrale Lille, ENSCL, Univ. Artois, UMR 8181—UCCS—Unité de Catalyse et Chimie du Solide, F-59000 Lille, France; camila.ferraz@univ-lille.fr (C.P.F.); sebastien.paul@centralelille.fr (S.P.)

2 Departamento de Química Fundamental, Instituto de Química, Universidade de São Paulo, Av. Prof. Lineu Prestes, 748, São Paulo-SP 05508-000, Brazil; andersondeob@gmail.com (A.G.M.D.S.); thenner07@yahoo.com.br (T.S.R.); camargo@iq.usp.br (P.H.C.C.)

* Correspondence: robert.wojcieszak@univ-lille.fr; Tel.: +33-320-335-438

Received: 19 June 2018; Accepted: 24 July 2018; Published: 27 July 2018

Featured Application: The catalysts developed in this work could be potentially used industrially for green oxidations of bio-based compounds.

Abstract: A series of catalysts consisting of gold nanoparticles supported on MnO_2 presenting different morphologies were synthesized and tested in the base-free oxidation of furfural. Ultra-small Au particles (less than 3 nm) were deposited on low (commercial MnO_2) and high (NF, nanoflowers and NW, nanowires MnO_2) surface area supports. High activity was observed for Au/MnO_2-NF material with very high selectivity to furoic acid. The X-ray photoelectron spectroscopy (XPS) study confirmed the presence of a significant amount of highly active $Au^{\delta+}$ species on the surface of the Au/MnO_2-NF catalyst. These species seem to be responsible for the high activity in oxidation of furfural under mild conditions (air as oxidant, 110 °C).

Keywords: gold nanoparticles; oxidation; MnO_2; nanoflowers

1. Introduction

In recent decades, supported gold nanoparticles have been extensively studied because of their unusual catalytic properties [1–4]. It is well recognized that the size of gold nanoparticles determines both the activity and the selectivity of the final catalyst [4,5]. It is also considered that the drastic change of the catalytic properties of nanoparticles is due to their new properties (physical and chemical) which are created when their size decreases, mainly due to the significant increase in the number of atoms on the surface [5–7]. However, when working with supported gold nanoparticles (NPs), the support also plays a very important role. Supported gold nanoparticles should be well dispersed to be able to interact with the support. Appropriate support can increase the dispersion of gold NPs, and hence improve the overall catalytic activity [8]. For Au catalysts supported on reducible supports, such as Fe_2O_3, TiO_2, CeO_2, and MnO_2, the dominant reaction pathway is expected to involve adsorption of a molecular oxygen species on the support, its dissociation at the interface, and then its reaction with the substrate [9]. In the case of Au supported on inert oxides (SiO_2 or Al_2O_3), the oxygen supply most likely proceeds via direct dissociative adsorption on the Au particles. The influence of the support on the catalytic activity strongly depends on the type of catalyzed reaction [10]. Ishida et al. [11] studied the effect of supported gold catalyst on the catalytic oxidation of glucose. They found that compared to gas phase catalytic oxidation reactions (such as for instance oxidation of CO), in the liquid phase oxidation,

the influence of gold particle size is more important than the nature of the support. Commoti et al. [12] observed similar results. They have also stated that the size of the Au particles appears to be the most important parameter. However, in these studies, the oxidation was always performed at high pH [12]. Indeed, the majority of works in the literature deal with the oxidation of sugars or of other bio-based compounds at controlled basic pH. At this pH, the substrates were almost always completely converted [13]. Moreover, several papers reported the need for a basic medium to perform the selective oxidation [12–15]. According to them, the presence of a base allows higher reaction rates, higher feed concentrations, better product solubility and lower adsorption of the products on the catalyst surface. However, oxidation in the liquid phase may occur at the interface between Au particles and the support. In this case, the activation energy would be different, depending on the nature of the support. Metal-oxide support interactions might affect Au clusters electronically and lead to weaker rate dependencies than those observed for unsupported Au nanoparticles. Obviously, the metal-support interactions depend on the nature of the support and of its structure [16]. It would be preferable to study the support effects without using basic conditions. Indeed, in the high pH range, the base used for the reaction governs the mechanism of the reaction. There is no systematic study in the literature which establishes a correlation between the support structure interacting with gold nanoparticles and their catalytic activity and selectivity. Therefore, we attempted to study the catalytic performance of supported gold nanoparticles for the base-free oxidation of furfural, using different manganese oxide structures (MnO_2) as supports. Firstly, the oxidation of furfural can lead to interesting products, such as 2-furoic [17] or maleic acid [18]. Indeed, 2-furoic acid can undergo a C-H carboxylation with CO_2 to form 2,5-furanodicarboxylic acid (FDCA) [19]. Secondly, MnO_2 is one of the most attractive materials because of its technological importance and possible application in different catalytic and electrochemical processes [20]. Moreover, the properties of MnO_2 are significantly influenced by its structure and morphology, which permits the study of the effect of the support structure on the catalytic activity. Therefore, we report herein about catalysts composed of MnO_2 with different structures modified with very small gold nanoparticles. Prepared materials were studied in the liquid phase oxidation of furfural using air (or oxygen) as the oxidant and water as the solvent.

2. Materials and Methods

2.1. Materials

Analytical grade chemicals chloroauric acid trihydrate ($HAuCl_4 \cdot 3H_2O$, 99.9%, Sigma-Aldrich, St. Louis, MO, USA), manganese sulfate monohydrate ($MnSO_4 \cdot H_2O$, 99%, Sigma-Aldrich, St. Louis, MO, USA), potassium permanganate ($KMnO_4$, 99%, Sigma-Aldrich, St. Louis, MO, USA), ethylene glycol (EG, 99,8%, Sigma Aldrich, St. Louis, MO, USA), sodium borohydride ($NaBH_4$, 98%, Sigma-Aldrich, St. Louis, MO, USA), polyvinylpyrrolidone (PVP, Sigma-Aldrich, St. Louis, MO, USA, M.W. 55,000 g/mol), manganese oxide (MnO_2, ReagentPlus®, St. Louis, MO, USA, ≥99%, Sigma-Aldrich—further noted MnO_2-Comm), furfural ($C_5H_4O_2$, > 99%, Sigma-Aldrich, St. Louis, MO, USA) were used as received. All solutions were prepared using deionized water (18.2 MΩ).

The MnO_2 nanoflowers (MnO_2-NF) and nanowires (MnO_2-NW) were obtained by a hydrothermal approach, as described elsewhere [21]. In a typical procedure for the synthesis of nanoflowers, 0.4 g of $MnSO_4$. H_2O and 1.0 g of $KMnO_4$ were dissolved in 30 mL of deionized water. This solution was transferred to a 100 mL Teflon-lined stainless-steel autoclave. The autoclave was heated and stirred at 140 °C for 1 h and then allowed to cooled down to room temperature. For the synthesis of MnO_2 nanowires, the same procedure was employed, but the autoclave was heated and stirred at 140 °C for 18 h. The products were collected by centrifugation and washed three times with ethanol (15 mL) and three times with water (15 mL) by successive rounds of centrifugation and removal of the supernatant. As-prepared materials were then dried at 80 °C for 6 h in air.

The supported gold nanoparticles were prepared as follow: Typically, 200 mg of MnO_2 support and 260 mg of PVP were added to 200 mL of EG. The obtained suspension was transferred to a 25 mL

round-bottom flask and kept under vigorous stirring at 90 °C for 20 min. Then, 3.0 mL of a 120 mM $NaBH_{4(aq)}$ and 3 mL of a 24 mM $AuCl_4^-{}_{(aq)}$ solutions were sequentially added to the reaction flask. This mixture was kept under vigorous stirring for another 1 h to produce Au/MnO_2. After cooling down to room temperature, the Au/MnO_2 materials were isolated by centrifugation and washed three times with acetic acid (15 mL), three times with ethanol (15 mL), and three times with water (15 mL) by successive rounds of centrifugation at 6000 rpm for 5 min and removal of the supernatant. After washing, the Au/MnO_2 materials were dried at 120 °C for 6 h in air.

2.2. Characterization

The transmission electron microscopy (TEM) and high-resolution transmission electron microscopy (HRTEM) images were obtained with a JEOL JEM2100 microscope (JEOL USA, Peabody, MA, USA) operated at 200 kV. High angle annular dark field (HAADF) and energy dispersive X-ray spectroscopy (EDS) images were acquired using a FEI TECNAI G2 F20 (The Ames Laboratory, Ames, IA, USA) operated at 200 kV. Samples for HRTEM, HAADF-STEM (High-angle annular dark-field scanning transmission electron microscopy), and EDX-STEM (Energy-dispersive X-ray spectroscopy scanning transmission electron microscopy) were prepared by drop-casting an aqueous suspension of the nanostructures over a carbon-coated copper grid, followed by drying under ambient conditions. The Au atomic percentage was measured by flame atomic absorption spectrometry (FAAS) with a Shimadzu spectrophotometer, model AA-6300 (Shimadzu Corp., Kyoto, Japan), equipped with an air-acetylene flame. Leaching tests were performed using ICP-OES (Inductively Coupled Plasma Optical Emission Spectrometry). An Agilent 720-ES ICP-OES (Agilent Technologies, Santa Clara, CA, USA) was used for determining the elemental composition of the reactant solutions.

Temperature-programmed reduction with hydrogen (H_2-TPR) was carried out in a Micrometrics Chemisorb 2705. Usually, 0.1 g of a catalyst was dried with N_2 flow at 125 °C for 1 h. Then, the sample was cooled down to room temperature, and then reduced up to 1000 °C (ramp 5·°C·min^{-1}) under H_2 flow (30 mL·min^{-1}). X-ray photoelectron spectroscopy (XPS) data of the samples were obtained with a SPECSLAB II (Phoibos-Hsa 3500 150, 9 channeltrons) SPECS spectrometer, with Al Kα source (E = 1486.6 eV) operating at 12 kV, pass energy (Epass) = 40 eV, 0.1 eV energy step and an acquisition time of 1 s per point. The samples were placed on stainless-steel sample-holders, transferred under inert atmosphere to the XPS pre-chamber and held there for 2 h in a vacuum. The residual pressure inside the analysis chamber was ~1×10^{-1} Torr. The binding energies (BE) of the Mn 2p, Au 4f and C 1s spectral peaks were referenced to the C 1s peak at 284.5 eV, providing accuracy within $\pm$ 0.2 eV. Textural characteristics of the catalysts were determined from nitrogen adsorption isotherms, recorded at −196 °C in a Quantachrome Nova 1000. The samples (ca. 100 mg) were degassed for 3 h at 150 °C before analysis. Specific surface areas were determined by the Brunauer-Emmett-Teller equation (BET method) from an adsorption isotherm generated in a relative pressure range $0.07 < P/Po < 0.3$. The total pore volume was calculated from the amount of N_2 adsorbed at a relative pressure close to unity. The average pore diameter was determined by the Barrett-Joyner-Halenda (BJH) method, from the N_2 desorption isotherms.

2.3. Catalytic Tests

Furfural oxidation was carried out on the REALCAT platform [22] in a Screening Pressure Reactors system (SPR) from Unchainedlabs, equipped with 24 parallel batch reactors for high-throughput screening of the catalytic materials. The catalysts (10 mg) were placed in each reactor. Then, 3 mL of an aqueous solution of furfural (1.0 wt %) was injected. The catalytic tests were performed under air (12 bar) for 2 h at 110 °C under acidic pH (pH = 3). After the reactions, the reactors were cooled down to room temperature. The liquid products were analyzed by High Performance Liquid Chromatography (HPLC, Waters 2410 RJ) equipped with RI and UV detectors and a Shodex SUGARSH-1011 column (8 × 300 mm). Diluted H_2SO_4 (5 mM, 1 mL/min) was used as a mobile phase. Commercial standards (furoic acid, furfural) were used for calibration of the HPLC set up. The recyclability tests were

done in the same reaction conditions. Temperature, initial pressure, air atmosphere, duration of the reaction, catalyst amount and initial reactant concentration were set as follow: 110 °C, 12 bar, air, 2 h, furfural:Au ratio of 100:1. After the first run, the reactant solution was taken out from the reactor using a syringe. The catalyst was recovered by centrifugation, and then dried at 100 °C overnight. The next day, the second run was performed. The same amount of catalyst was weighed and added to the reactor. After that, the reactor was closed, and the test was performed again in the same conditions as previously used.

3. Results

In order to characterize the materials, several techniques have been used: HRTEM, FAAS and XPS. It is already well established that the catalytic activity of the supported gold catalysts strongly depends on the average Au particle size. HRTEM measurements were applied to determine the exact size distribution of the synthesized gold nanoparticles. In our case, the strategy was to prepare, on different supports, ultra-dispersed gold nanoparticles with similar average particle size, using PVP as a stabilizer and $NaBH_4$ as a reductant. Indeed, this method is generally applied for the synthesis of nanometric metallic nanoparticles [23].

3.1. Structural properties

TEM images of the Au/MnO_2-MF, Au/MnO_2-NW and Au/MnO_2-Comm materials obtained by this route are shown in Figure 1. The Au NPs deposited on the different supports were monodispersed, and had very small sizes of about 2.6 nm (±0.8 nm) in all cases. Moreover, as could be seen, Au nanoparticles were uniformly dispersed onto the MnO_2 surfaces. In addition, no significant agglomeration of gold nanoparticles was detected.

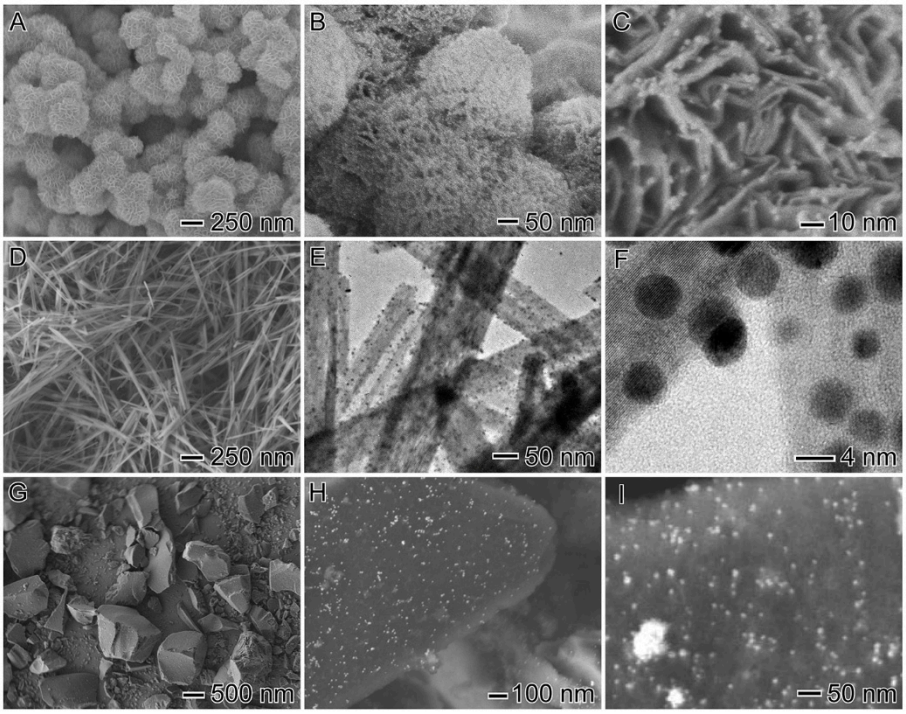

Figure 1. TEM images of the Au/MnO_2-NF catalysts (**B**,**C**), Au/MnO_2-NW (**E**,**F**) and Au/MnO_2-Comm (**H**,**I**) catalysts. Images (**A**,**D**,**G**) represent MnO_2-NF, MnO_2-NW and MnO_2-Comm bare supports, respectively. Images (**C**,**H**,**I**) represent HAADF-STEM images.

The different morphologies of the three different MnO_2 supports used were clearly observed in the TEM images. Moreover, significant differences were also observed in the specific surface areas of these materials, as can be seen in Table 1.

Table 1. Au wt %, Au gold particle size, BET surface area, pore volume and pore diameter determined by FAAS, TEM and BET - N_2 adsorption, respectively.

Catalyst	Au (wt %)	Particle size (nm)	Surface Area (m^2/g)	Pore Volume (cm^3/g)	Pore Diameter (Å)
Au/MnO_2-NF	1.3	2.6	196	0.42	6.1
MnO_2 NF	-	-	194	0.41	6.1
Au/MnO_2-NW	1.3	3.2	125	0.16	6.9
MnO_2-NW	-	-	122	0.16	6.8
Au/MnO_2-Comm	1.4	2.6	15	0.05	17.8
MnO_2-Comm	-	-	14	0.05	17.8

The specific surface areas of both homemade MnO_2 supports (MnO_2-NF and MnO_2-NW) are roughly ten times as high as that of the commercial oxide (MnO_2-Comm). The nanoflowers MnO_2 presented the highest surface, and also pore volume (Table 1). These characteristics could strongly influence the activity of this material. Moreover, the modification of the MnO_2 materials with gold nanoparticles did not change the structural and morphological properties of the bare support. Indeed, as could be expected, high dispersion of the gold nanoparticles permitted a slight increase in the overall specific surface areas of the prepared catalysts. It is interesting to note that the huge differences in the surface areas of the commercial support and the homemade samples did not impact the average particle size of the gold nanoparticles (Table 1). Indeed, this was one of the objectives of this work, and it is due to the method of preparation of the Au particles using PVP as a stabilizer. Taking into account the same average Au particle size and metal loading, it seems that the catalytic performances should be governed mostly by the structure and the morphology of the support.

Interesting results were obtained from H_2-TPR studies (Figure 2). The reducibility of the MnO_2 support represents an important parameter in the context of catalytic applications. This is because Au NPs (active phase) can strongly interact with metal oxides and change their redox properties. This, in turn, can affect catalytic activity.

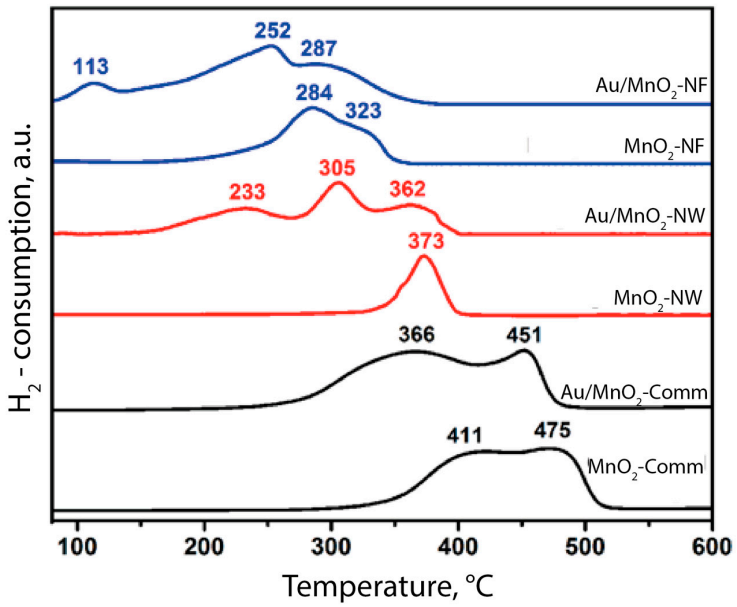

Figure 2. Temperature programmed reduction (TPR) profiles for MnO_2 nanoflowers (in blue), nanowires (in red), and commercial MnO_2 (in black) before and after the deposition of Au nanoparticles on their surfaces.

The TPR profile for MnO_2 nanoflowers displayed two peaks, centred at 284 and 323 °C, assigned to the reduction of MnO_2 to Mn_xO_y (displaying lower oxidation states) [24]. After the deposition of the ultra-small Au NPs at the nanoflowers' surface, a marked change in the TPR profile was observed. Indeed, the reduction of MnO_2 was shifted to lower temperatures, and three main reduction peaks corresponding to the reduction of Mn_3O_4 to MnO (113 °C), Mn_2O_3 to Mn_3O_4 (252 °C), and MnO_2 to Mn_2O_3 (287 °C) could be observed [24,25]. This effect may be due to strong metal-support interactions. Previous investigations suggested that the presence of small Au NPs can also facilitate the MnO_2 reduction [25]. Results obtained from H_2-TPR showed that high surface area support (MnO_2-NF) and smaller Au NPs led to stronger metal-support interactions, due to the higher interfacial perimeter between Au and the oxide support. The reduction of MnO_2 occurred, in this case, at lower temperature. In contrast, the low surface area support (MnO_2-comm) presents lower interaction between metal and oxide, and the presence of gold does not significantly change the high reduction temperature of this support.

3.2. Catalytic Activity

All prepared samples and bare supports were tested in the aqueous phase oxidation of furfural to furoic acid. Supports alone showed, already, a significant activity for this reaction (up to 55% furfural conversion in case of MnO_2-NF). However, the selectivity to furoic acid was much lower than in the case of Au-modified samples (c.a. 80%). It reached only 25% in the case of the MnO_2-NF sample at a furfural iso-conversion of 55%. It is well established that MnO_2 materials are good catalysts for oxidation reactions. Generally, oxidation of furfural to furoic acid is carried out in the presence of hazardous oxidants [26,27] or heterogeneous catalysts in a strong alkaline solution [28]. However, at alkaline pH, degradation of furfural can occur, resulting in a drop of selectivity. Furthermore, instead of leading to furoic acid salt, the oxidation reaction can yield mixtures of low and high molecular weight products. The basic medium is also related to degradation of furfural and the formation of other furan derivates (such as 5-HMF) under reaction conditions. Tests in absence of catalyst showed conversion without any detection of oxidation products. In addition, a colour change was noticed in the reaction mixture from yellow to brownish, with the formation of a black precipitate [29,30]. This precipitate was attributed to the formation of humic acids, which are a mixture of many different acids that can be formed during dehydration, and also arise from the condensation of furfural. The present study showed that working in base-free conditions is possible using highly selective supported gold nanoparticles. Figure 3 presents the results obtained for furfural oxidation with air at 110 °C. After only 2 h of reaction, Au/MnO_2-NF catalyst reached 86% of furfural conversion (Table 2, Entry 3). At the same time, Au supported on commercial MnO_2 oxide showed only 69% of conversion. In the case of both homemade catalysts (Au/MnO_2-NF and Au/MnO_2-NW), very high selectivity to furoic acid was obtained (more than 80%), and the carbon balance values indicated that no degradation of furfural occurred.

The most active Au/MnO_2-NF catalyst was tested in different reaction conditions, to optimize the furoic acid yield. As could be seen from Table 2, full furfural conversion was reached after 4 h of reaction at 110 °C (Entry 4). In addition, this catalyst was already active at lower temperatures, and 65% of conversion was obtained at 80 °C after 4 h of reaction. The best results were obtained at 110 °C and after 4 h of reaction. In these conditions, furoic acid can be produced with a yield of 82% (Entry 4).

The reaction temperature strongly affects the catalytic properties of the supported gold nanoparticles. Indeed, at low temperature, high selectivity could be obtained, whereas high temperature favoured the degradation of furfural. Full conversion was observed at 150 °C (Entry 7), but only 67% of selectivity to furoic acid and a very low carbon balance, ascribed to the formation of undetected degradation products. Alternatively, for all the tests carried out in the 80–110 °C temperature range, high values of carbon balance were observed, which suggests that no degradation of furfural took place (Entries 1–6). In addition, ICP analysis of post-reactant mixtures confirmed that

no Au leaching occurred. However, a low quantity of Mn^{2+} was detected in the solution, indicating low Mn^{2+} leaching (12–14 ppm). Taking into account the Mn^{2+} leaching, recycling tests were performed. Spent catalysts were also studied by TEM, as reported in the next section.

Catalyst reuse was tested on all catalysts. The results are given in Table 3.

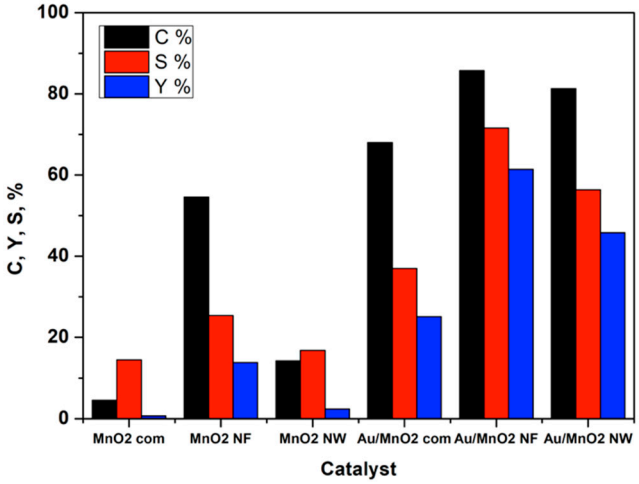

Figure 3. The furfural oxidation reaction on different MnO_2 oxides and Au modified samples: P = 12 bar (air), T = 110 °C, reaction time 2 h, furfural:Au molar ratio = 100:1. C stands for the furfural conversion, S for the selectivity in furoic acid and Y for the yield of furoic acid, respectively.

Table 2. Screening of the catalytic conditions using Au/MnO_2-NF catalyst. P = 12 bar (air), furfural:Au molar ratio = 100:1.

Entry	T [°C]	Time [min]	X_{FUR} [%]	S_{FA} [%]	CB [%]
1	110	30	45	82	93
2	110	70	61	80	93
3	110	120	86	72	92
4	110	240	100	82	93
5	80	120	31	92	92
6	80	240	65	89	96
7	150	120	100	67	75

Table 3. Recycling tests. P = 12 bar (air), T = 110 °C, reaction time 2 h, furfural:Au molar ratio = 100:1.

Entry	Catalyst	X_{FUR} [%]	S_{FA} [%]	CB [%]
1	Au/MnO_2 -NF	82	74	92
2	Au/MnO_2-NW	75	64	93
3	Au/MnO_2-Comm	53	37	91

As can be seen, no significant decrease of the activity was observed. Only in the case of the Au/MnO_2-comm sample was the decrease of furfural conversion about 20%. This could be due to the increase of the Au particle size observed in TEM after the tests (section below). In the case of the Au/MnO_2-MF and Au/MnO_2-NW samples, no changes were observed as compared to the results reported in Figure 3.

3.3. Post-Test Characterization

In order to check the mechanical and textural stability of the catalysts, TEM studies were also carried out on spent catalysts (Figure 4A–F).

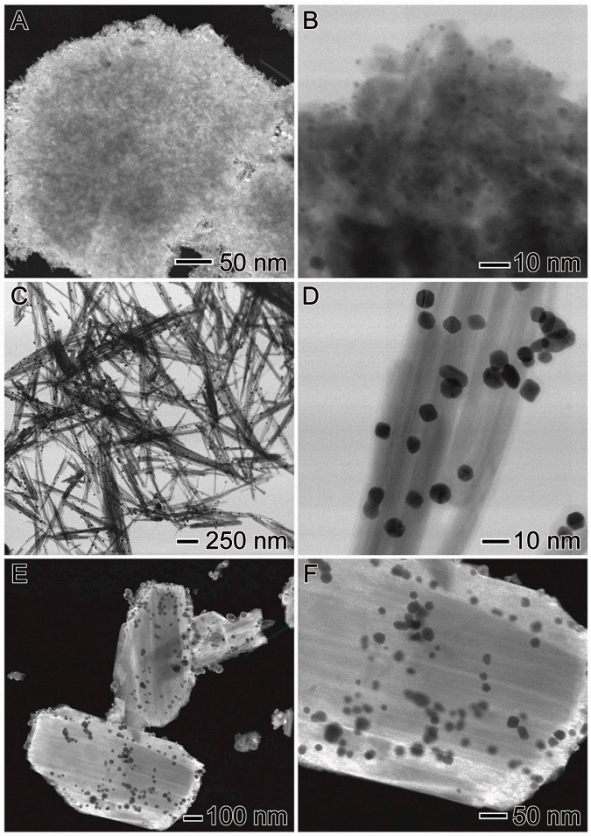

Figure 4. TEM studies of the spent catalysts: Au/MnO_2-NF (**A**,**B**), Au/MnO_2-NW (**C**,**D**) and Au/MnO_2-Comm (**E**,**F**).

As can be seen from Figure 4C–F, the structure of the Au/MnO_2-NW and Au/MnO_2-Comm samples are preserved. However, an increase in the Au particle size was observed in both cases. Specifically, the Au NPs sizes corresponded to 3.3 ± 0.9 nm and 16 ± 4 nm in diameter in the catalyst containing MnO_2 nanowires and commercial MnO_2, respectively. In the case of the Au/MnO_2-NF sample (Figure 4A,B), the structure of the support and average Au particle size were conserved. This indicates a better stability of this catalyst when compared to commercial and NW-based samples.

4. Discussion

As can be seen from the results presented above, the activity of the Au-based catalysts supported on MnO_2 strongly depends on the structure and morphology of the MnO_2 oxide used for the synthesis. It seems that it is not only the differences in surface area and pore volume that are responsible for the high activity of the MnO_2-NF catalyst. Even if, as could be seen from Table 1, the Au/MnO_2-NF material has significantly higher surface area than the MnO_2-Comm catalyst, the Au particle size did not change at all in both cases. This result differs from that observed in the literature. Indeed, Zhu et al. [31] studied different Au/MnO_2 materials in 5-HMF oxidation in an organic solvent. They observed that higher surface area was beneficial to obtain smaller Au particle sizes. However, in that case, the Au particle sizes were quite large (between 6 and 20 nm), which could explain the differences in the activity observed by the authors. In our study, all materials have similar Au particle size (about 3 nm), which suggests that only the structure of the support governs the catalytic activity. To better understand the differences, we decided to study in more detail the Mn and Au surface species present in the catalysts. X-ray photoelectron spectroscopy (XPS) is a powerful tool to study the external surface of catalysts, and is able to determine the chemical composition and oxidation states of the components present on the catalyst surface. In the case of the MnO_2 nanoflowers support, one main

photoelectron peak at the Mn $2p_{3/2}$ region centred at 642.6 eV, which can be assigned to the presence of Mn^{4+} species, was observed. Moreover, after the deposition of small gold nanoparticles, changes in the oxidation state of the Mn species occurred (Table 4). The main peak in the Mn $2p_{3/2}$ region was broadened and shifted to 641.7 eV. This could indicate the partial reduction of Mn^{4+} to $Mn^{\delta+}$ ($\delta < 4$) at the surface. Concerning the O 1s XPS region, three different surface oxygen species could be identified. The binding energy between 529.9–529.5 eV was characteristic of the lattice oxygen (denoted as O_L), the binding energies between 532.0–531.4 eV were assigned to oxygen vacancies or the surface oxygen ions (denoted as O_s), and the binding energies around 533.9 eV were characteristic of adsorbed water. In addition, incorporation of Au NPs to the MnO_2 nanoflowers material led to a more significant decrease in the O_L/O_s ratio as compared to the pure MnO_2 nanoflowers. This demonstrates that the enrichment of oxygen vacancies or the surface oxygen ions was induced by the partial reduction of Mn^{4+} species during the Au NPs deposition step. At the same time, the extent of $Au^{\delta+}$ species increases for the MnO2-NF sample, indicating higher numbers of gold active sites.

Table 4. Binding energies measured by XPS before and after the deposition of Au NPs at the surface of the different MnO_2 supports (OL—lattice oxygen species, OS—oxygen ions).

Sample	BE of Mn 2p3/2 (eV)	BE of O 1s (eV)		Au 4f (eV)
		OL	OS	$Au^{\delta+}$
Au/MnO_2-NW	641.7	530.1 (46) *	532.0 (39) *	85.4 (20) *
MnO_2-NW	642.6	529.5 (52) *	531.5 (34) *	no signal
Au/MnO_2-comm	642.0	530.1 (56) *	532.0 (30) *	86.5 (18) *
MnO_2-comm	642.7	530.0 (56) *	532.2 (29) *	no signal
Au/MnO_2-NF	641.7	529.8 (41) *	531.6 (47) *	85.5 (26) *
MnO_2-NF	642.6	530.0 (61) *	532.0 (28) *	no signal

* % of O or Au species.

At the same time, the XPS Au 4f region displayed broad peaks (Figure 5C), suggesting the presence of different oxidation states of gold (Au^0 and $Au^{\delta+}$ species).

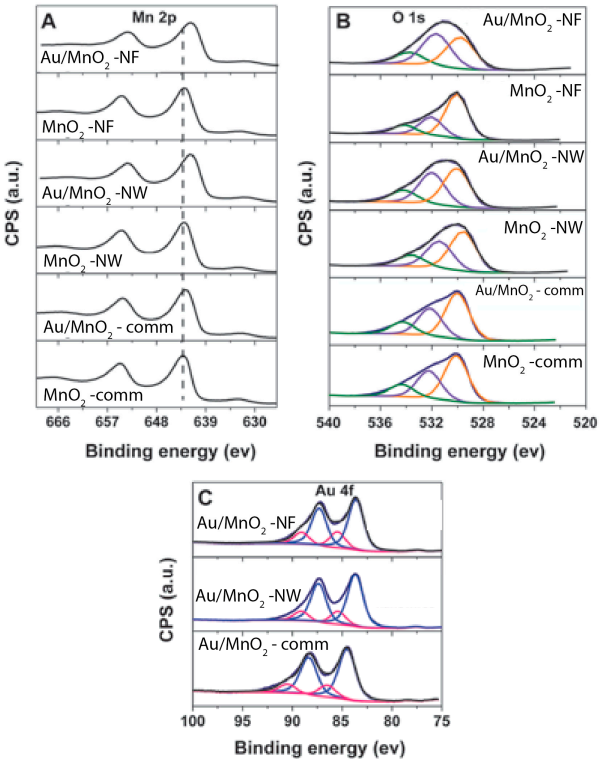

Figure 5. XPS spectra of Mn 2p (**A**), O 1s (**B**) and Au 4f (**C**) regions for the prepared catalysts.

As observed in Table 4, the deposition of Au NPs on MnO_2 supports led to the formation of a significant amount of $Au^{\delta+}$ species. Specifically, the $Au^{\delta+}$ species ratio was ~26 % in Au/MnO_2-NF, which is a higher proportion in comparison with the other supports. This could be responsible for the enhanced catalytic activity of this catalyst. Indeed, previous works on supported Au nanoparticles has indicated surface $Au^{\delta+}$ species as being the most catalytically active sites in oxidation reactions [25,32].

5. Conclusions

We have studied different Au/MnO_2 systems in the base-free oxidation of furfural to furoic acid. Small Au nanoparticles of the same size were deposited on three different MnO_2 materials, which permitted the study of the effects of the morphology and metal-support interaction on catalytic activity. The best results were obtained using a homemade nanostructured support (MnO_2-NF). This catalyst showed not only the best morphological properties (high surface area, high pore volume), but also excellent catalytic properties (high furfural conversion, optimal selectivity). The differences in the catalytic results were assigned to the presence of a significant amount of $Au^{\delta+}$ species on the surface, as shown by XPS. Indeed, the $Au^{\delta+}$ species present in MnO_2-NF material are indicated as being the most catalytically active sites in oxidation reactions.

Author Contributions: R.W., C.P.F and A.G.M.D.S. and T.S.R. conceived and designed the experiments; A.G.M.D.S. and C.P.F. performed the experiments; R.W., P.H.C.C., S.P. and T.S.R. analyzed the data; R.W., P.H.C.C. and S.P. wrote the paper.

Funding: This work was done in the frame of the LIA "Energy&Environment" funded by CNRS.

Acknowledgments: The REALCAT platform is benefiting from a state subsidy administrated by the French National Research Agency (ANR) within the frame of the 'Investments for the Future' program (PIA), with the contractual reference 'ANR-11-EQPX-0037'. The European Union, through the ERDF funding administered by the Hauts-de-France Region has co-financed the platform. Centrale Lille, CNRS, and the University of Lille, as well as the Centrale Initiatives Foundation, are thanked for their financial contributions to the acquisition and implementation of the equipment of the REALCAT platform. The authors acknowledge support from FAPESP (Grant numbers No. 2015/50010-8, 15/26308-7, and 2017/03235-0).

Conflicts of Interest: The authors declare no conflict of interest.

References

1. Kumar, R.; Gravel, E.; Hagege, A.; Li, H.; Jawale, D.V.; Verma, D.; Namoboothiri, I.N.N.; Doris, E. Carbon nanotube-gold nanohybrids for selective catalytic oxidation of alcohols. *Nanoscale* **2013**, *5*, 6491–6497. [CrossRef] [PubMed]
2. Wojcieszak, R.; Ferraz, C.P.; Sha, J.; Houda, S.; Rossi, L.M.; Paul, S. Advances in Base free oxidation of bio-based compounds on supported gold catalysts. *Catalysts* **2017**, *7*, 352–375. [CrossRef]
3. Wojcieszak, R.; Cuccovia, I.M.; Silva, M.A.; Rossi, L.M. Selective oxidation of glucose to glucuronic acid by cesium-promoted gold nanoparticle catalyst. *J. Mol. Catal. A Chem.* **2016**, *422*, 35–42. [CrossRef]
4. Solmi, S.; Morreale, C.; Ospitali, F.; Agnoli, S.; Cavani, F. Oxidation of d-glucose to glucaric acid using Au/C catalysts. *ChemCatChem* **2017**, *9*, 2797–2806. [CrossRef]
5. Haruta, M. When Gold Is Not Noble: Catalysis by Nanoparticles. *Chem. Rec.* **2003**, *3*, 75–87. [CrossRef] [PubMed]
6. Murray, C.B.; Norris, D.J.; Bawendi, M.G. Synthesis and characterization of nearly monodisperse CdE (E = sulfur, selenium, tellurium) semiconductor nanocrystallites. *J. Am. Chem. Soc.* **1993**, *115*, 8706–8715. [CrossRef]
7. Gonçalves, R.; Vono, L.; Wojcieszak, R.; Dias, C.; Wendere, H.; Teixeira-Neto, E.; Rossi, L. Selective hydrogenation of CO2 into CO on a highly dispersed nickel catalyst obtained by magnetron sputtering deposition: A step towards liquid fuels. *Appl. Catal. B* **2017**, *209*, 240–246. [CrossRef]
8. Önal, Y.; Schimpf, S.; Claus, P. Structure sensitivity and kinetics of d-glucose oxidation to d-gluconic acid over carbon-supported gold catalysts. *J. Catal.* **2004**, *223*, 122–133. [CrossRef]

9. Stephen, A.; Hashmi, K. Gold-Catalyzed Organic Reactions. *Chem. Rev.* **2007**, *107*, 3180–3211. [CrossRef]
10. Okatsu, H.; Kinoshita, N.; Akita, T.; Ishida, T.; Haruta, M. Deposition of gold nanoparticles on carbons for aerobic glucose oxidation. *Appl. Catal. A* **2009**, *369*, 8–14. [CrossRef]
11. Ishida, T.; Kinoshita, N.; Okatsu, H.; Akita, T.; Takei, T.; Haruta, M. Influence of the Support and the Size of Gold Clusters on Catalytic Activity for Glucose Oxidation. *Angew. Chem. Int. Ed.* **2008**, *120*, 9405–9408. [CrossRef]
12. Comotti, M.; Pina, C.D.; Matarrese, R.; Rossi, M.; Siani, A. Oxidation of alcohols and sugars using Au/C catalysts: Part 2. *Sugars. Appl. Catal. A* **2005**, *291*, 204–209. [CrossRef]
13. Eggleston, G.; Vercellotti, J.R. Degradation of Sucrose, Glucose and Fructose in Concentrated Aqueous Solutions Under Constant pH Conditions at Elevated Temperature. *Carbohydr. Res.* **2000**, *19*, 1305–1318. [CrossRef]
14. Biella, S.; Prati, L.; Rossi, M. Selective Oxidation of D-Glucose on Gold Catalyst. *J. Catal.* **2002**, *206*, 242–247. [CrossRef]
15. Comotti, M.; Della Pina, C.; Matarrese, R.; Rossi, M. The catalytic activity of "naked" gold particles. *Angew. Chem. Int. Ed.* **2004**, *43*, 5812–5815. [CrossRef] [PubMed]
16. Bettahar, M.; Wojcieszak, R.; Monteverdi, S. NiAg catalysts prepared by reduction of Ni2+ ions in aqueous hydrazine II. Support effect. *J. Colloid Interface Sci.* **2009**, *332*, 416–424. [CrossRef] [PubMed]
17. Gupta, N.; Fukuoka, A.; Nakajima, K. Metal-free and selective oxidation of furfural to furoic acid with an N-heterocyclic carbene catalyst. *ACS Sus. Chem. Eng.* **2018**, *6*, 3434–3442. [CrossRef]
18. Wojcieszak, R.; Santarelli, F.; Paul, S.; Dumeignil, F.; Cavani, F.; Gonçalves, R.V. Recent developments in maleic acid synthesis from bio-based chemicals. *Sustain. Chem. Process.* **2015**, *3*, 9–20. [CrossRef]
19. Banerjee, A.; Dick, G.; Yoshino, T.; Kanan, M. Carbon dioxide utilization via carbonate-promoted C–H carboxylation. *Nature* **2016**, *531*, 215–219. [CrossRef] [PubMed]
20. Hayashi, E.; Komanoya, T.; Kamata, K.; Hara, M. Heterogeneously-Catalyzed Aerobic Oxidation of 5-Hydroxymethylfurfural to 2,5-Furandicarboxylic Acid with MnO2. *ChemSusChem* **2017**, *22*, 654–658. [CrossRef] [PubMed]
21. Wang, X.; Li, Y. Selected-Control Hydrothermal Synthesis of α- and β-MnO2 Single Crystal Nanowires. *J. Am. Chem. Soc.* **2002**, *124*, 2880–2881. [CrossRef] [PubMed]
22. Realcat Platform. Available online: www.realcat.fr (accessed on 25 May 2018).
23. Deraedt, Ch.; Salmon, L.; Gatard, S.; Ciganda, R.; Hernandez, R.; Ruiz, J.; Astruc, D. Sodium borohydride stabilizes very active gold nanoparticle catalysts. *Chem. Commun.* **2014**, *50*, 14194–14196. [CrossRef] [PubMed]
24. Wang, L.-C.; Liu, Y.-M.; Chen, M.; Cao, Y.; He, H.Y.; Fan, K.-N. MnO_2 Nanorod Supported Gold Nanoparticles with Enhanced Activity for Solvent-free Aerobic Alcohol Oxidation. *J. Phys. Chem. C* **2008**, *112*, 6981–6987. [CrossRef]
25. da Silva, A.G.M.; Kisukuri, C.M.; Rodrigues, T.S.; Candido, E.G.; de Freitas, I.C.; da Silva, A.H.M.; Assaf, J.M.; Oliveira, D.C.; Andrade, L.H.; Camargo, P.H.C. MnO_2 nanowires decorated with Au ultrasmall nanoparticles for the green oxidation of silanes and hydrogen production under ultralow loadings. *Appl. Catal. B* **2016**, *184*, 35–43. [CrossRef]
26. Zeitsch, K.J. *The Chemistry and Technology of Furfural and Its Many By-Products*; Elsevier: Amsterdam, The Netherlands, 2000; pp. 159–163. ISBN 9780444503510.
27. Taarning, E.; Nielsen, I.S.; Egeblad, K.; Madsen, R.; Christensen, C.H. Chemicals from Renewables: Aerobic Oxidation of Furfural and Hydroxymethylfurfural over Gold Catalysts. *ChemSusChem* **2008**, *1*, 75–78. [CrossRef] [PubMed]
28. Douthwait, M.; Huang, X.; Iqbal, S.; Miedziak, P.J.; Brett, G.L.; Kondrat, S.A.; Edwards, J.K.; Sankar, M.; Knight, D.W.; Bethell, D.; Hutchings, G.J. The controlled catalytic oxidation of furfural to furoic acid using AuPd/$M(OH)_2$. *Catal. Sci. Technol.* **2017**, *7*, 5284–5293. [CrossRef]
29. Vuyyuru, K.R.; Strasser, P. Oxidation of biomass derived 5-hydroxymethylfurfural using heterogeneous and electrochemical catalysis. *Catal. Today* **2012**, *195*, 144–154. [CrossRef]
30. Piccolo, A.; Conte, P.; Cozzolino, A. Effects of mineral and monocarboxylic acids on the molecular association of dissolved humic substances. *Eur. J. Soil Sci.* **1999**, *50*, 687–694. [CrossRef]

31. Zhu, Y.; Shen, M.; Xia, Y.; Lu, M. Au/MnO_2 nanostructured catalysts and their catalytic performance for the oxidation of 5-(hydroxymethyl)furfural. *Catal. Commun.* **2015**, *64*, 37–43. [CrossRef]
32. Yang, M.; Allard, L.F. Flytzani-Stephanopoulos, Atomically Dispersed Au–(OH)x Species Bound on Titania Catalyze the Low-Temperature Water-Gas Shift Reaction M. *J. Am. Chem. Soc.* **2013**, *135*, 3768–3771. [CrossRef] [PubMed]